

GA-A26783

# DEPENDENCE OF TRANSPORT ON THE SAFETY FACTOR PROFILE IN DIII-D STEADY-STATE SCENARIOS

by

C.T. HOLCOMB, J.R. FERRON, A.E. WHITE, T.C. LUCE, J.C. DeBOO,  
T.L. RHODES, L. SCHMITZ, and F. TURCO

MAY 2010



## **DISCLAIMER**

This report was prepared as an account of work sponsored by an agency of the United States Government. Neither the United States Government nor any agency thereof, nor any of their employees, makes any warranty, express or implied, or assumes any legal liability or responsibility for the accuracy, completeness, or usefulness of any information, apparatus, product, or process disclosed, or represents that its use would not infringe privately owned rights. Reference herein to any specific commercial product, process, or service by trade name, trademark, manufacturer, or otherwise, does not necessarily constitute or imply its endorsement, recommendation, or favoring by the United States Government or any agency thereof. The views and opinions of authors expressed herein do not necessarily state or reflect those of the United States Government or any agency thereof.

# DEPENDENCE OF TRANSPORT ON THE SAFETY FACTOR PROFILE IN DIII-D STEADY-STATE SCENARIOS

by

C.T. HOLCOMB,<sup>\*</sup> J.R. FERRON, A.E. WHITE,<sup>†</sup> T.C. LUCE, J.C. DeBOO,  
T.L. RHODES,<sup>‡</sup> L. SCHMITZ,<sup>‡</sup> and F. TURCO<sup>#</sup>

This is a preprint of a paper to be presented at the 37th European  
Physical Society Conference on Plasma Physics, June 21-25,  
2010, Dublin, Ireland and to be published in the *Proceedings*.

<sup>\*</sup>Lawrence Livermore National Laboratory, Livermore, California.

<sup>†</sup>Massachusetts Institute of Technology, Cambridge, Massachusetts.

<sup>‡</sup>University of California-Los Angeles, Los Angeles, California.

<sup>#</sup>Oak Ridge Institute for Science Education, Oak Ridge, Tennessee.

Work supported in part by  
the U.S. Department of Energy  
under DE-AC52-07NA27344, DE-FC02-04ER54698,  
and DE-FG03-08ER54984

GENERAL ATOMICS PROJECT 30200  
MAY 2010



## Dependence of Transport on the Safety Factor Profile in DIII-D Steady-state Scenarios

C.T. Holcomb<sup>1</sup>, J.R. Ferron<sup>2</sup>, A.E. White<sup>3</sup>, T.C. Luce<sup>2</sup>, J.C. DeBoo<sup>2</sup>, T.L. Rhodes<sup>4</sup>,  
L. Schmitz<sup>4</sup>, and F. Turco<sup>5</sup>

<sup>1</sup>*Lawrence Livermore National Laboratory, Livermore, California, 94551, USA*

<sup>2</sup>*General Atomics, PO Box 85608, San Diego, California 92186, USA*

<sup>3</sup>*Oak Ridge Institute for Science & Education, PO Box 117, Oak Ridge, Tennessee, 37831, USA*

<sup>4</sup>*University of California, Los Angeles, California 90095, USA*

<sup>5</sup>*Oak Ridge Associated Universities, PO Box 117, Oak Ridge, Tennessee 37831, USA*

### I. Introduction

Recent steady-state scenario experiments on DIII-D examined the complex and recursive relationship between the choice of target safety factor ( $q$ ) profile and the resulting transport, density and temperature profiles, and bootstrap current density at high noninductive current fraction [1]. This paper focuses on the transport and profile variation in a set of nine discharges in which the edge and minimum  $q$  ( $q_{95}$  and  $q_{\min}$ ) were scanned. These discharges were all ramped up to and held fixed at  $\beta_N = \beta_T(\%)/[I_p(MA)/a(m)B_T(T)] = 2.8$  using neutral beams under feedback control. The toroidal field  $B_T = 2.0$  Tesla, and the discharge shape was fixed to a slightly unbalanced double-null divertor, so  $q_{95}$  was varied by adjusting the plasma current  $I_p$ .  $q_{\min}$  was varied by adjusting the early-time power and H-mode transition time. Electron cyclotron current drive power was driven in a broad region centered at mid-radius to maintain broad, tearing mode-stable current profiles. The formation of deeply reversed magnetic shear and internal transport barriers was explicitly avoided in these experiments. No attempt was made to control the radius of  $q_{\min}$ .

The  $q$ -profiles were determined using the EFIT equilibrium reconstruction code [2] with the following constraints: edge magnetic sensors, motional Stark effect internal field pitch angle measurements [3], a pressure profile determined by measurements of density and temperature and a Monte Carlo calculation of the fast ion pressure (NUBEAM code [4]), and a pedestal current density set by the Sauter bootstrap current model [5] contained within the ONETWO transport code [6]. For each discharge, a period of 200 to 1200 ms was identified with  $\beta_N \approx 2.8$  and no large tearing modes present. All profiles shown here are the mean profile during this time period, and the error bars denote plus and minus one standard deviation. Stated values of  $q_{95}$  and  $q_{\min}$  are mean values in these periods. Most of this paper focuses on a comparison of the four discharges at the extremes of the  $q_{95}$  and  $q_{\min}$  scans, henceforth referred to as “the scan endpoints”. The same color-coding is used for these throughout: red is  $q_{95}=4.5$ ,  $q_{\min}=1.7$ , black is  $q_{95}=6.8$ ,  $q_{\min}=1.9$ , blue is  $q_{95}=4.5$ ,  $q_{\min}=1$ , and green is  $q_{95}=6.8$ ,  $q_{\min}=1$ . These  $q$ , density and temperature profiles are shown in Figs 1 and 2.

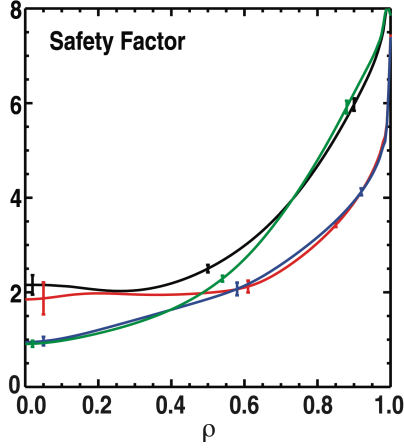


Fig. 1 Mean  $q$ -profiles produced in a scan of  $q_{95}$  and  $q_{min}$  at fixed  $\beta_N=2.8$  (4 scan endpoints shown).

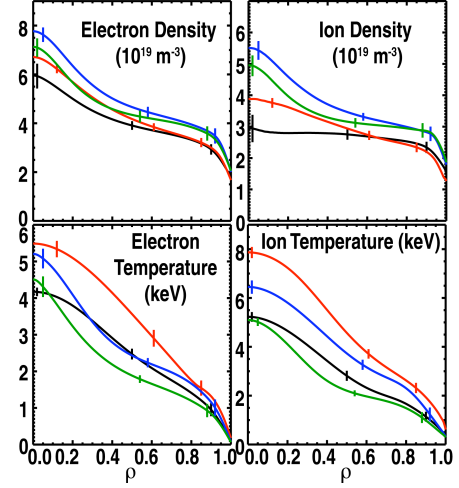


Fig. 2. Mean density and temperature profiles associated with the Fig. 1  $q$ -profiles (same color coding) shown systematic differences with  $q$ .

## II. Density and Temperature Profile Dependence on $q_{95}$ and $q_{min}$ at fixed $\beta_N=2.8$

Systematic differences with  $q_{95}$  and  $q_{min}$  greater than the one standard deviation are observed in electron density ( $n_e$ ) and temperature ( $T_e$ ), and ion density ( $n_i$ ) and temperature ( $T_i$ ). The core  $n_e$ ,  $T_e$ ,  $n_i$  and  $T_i$  all decrease with  $q_{95}$  in agreement with global energy confinement scaling with IP. At any  $q_{95}$ ,  $T_e$  and  $T_i$  increase with  $q_{min}$ . Increasing  $q_{min}$  broadens the  $T_e$  profile by increasing its gradient over the outer half-radius and decreasing it inside. The H-mode pedestal density decrease with  $q_{min}$  does not hold in general in the full 9-discharge dataset.

## III. Thermal Diffusivity and Power Balance Dependence on $q_{95}$ and $q_{min}$ at Fixed $\beta_N=2.8$

Thermal diffusivity ( $\chi$ ) profiles were calculated using ONETWO with the experimental profiles of current density, density, temperature, rotation, and radiated power as input, as well as the injected neutral beam and electron cyclotron heating power. Figures 3 and 4 show  $\chi_e$  and  $\chi_i$  for the scan endpoints. The maximum value of  $\chi_i$  near  $\rho=0.6-0.7$  increases with  $q_{95}$ , while  $\chi_e$  is less sensitive to  $q_{95}$ , especially at low  $q_{min}$ . The insets in Figs. 3 and 4 use the full 9-discharge data set and show variation of the mean  $\chi(\rho=0.7)$  with  $q_{95}$  and  $q_{min}$ .  $\chi_e$  generally decreases with  $q_{min}$ , while  $\chi_i$  stays the same or increases with  $q_{min}$ .

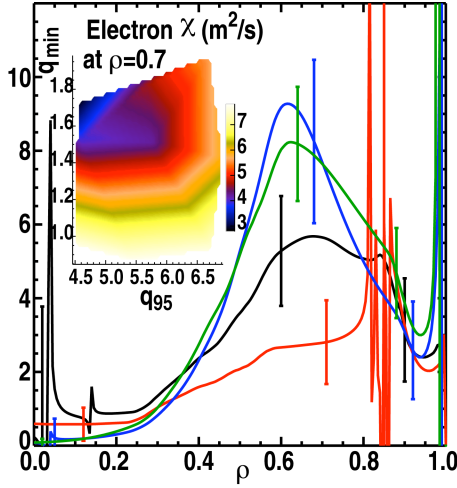


Fig. 3. Mean electron thermal diffusivity profiles (Fig. 1 color coding) and contours of  $\chi_e$  ( $\rho=0.7$ ) vs.  $q_{95}$  and  $q_{\min}$  using the full dataset (inset).

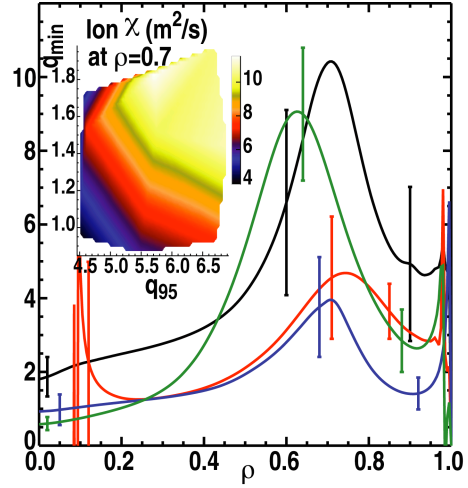


Fig. 4. Mean ion thermal diffusivity profiles (Fig. 1 color coding) and contours of  $\chi_i$  ( $\rho=0.7$ ) vs.  $q_{95}$  and  $q_{\min}$  using the full dataset (inset).

Figure 5 shows the power balance of the scan endpoints. The bars indicate mean power to (positive) or from (negative) ions (red) and electrons (blue) during the analysis time period. The categories are neutral beam injection (NBI), ion to electron exchange ( $i \rightarrow e$ ), conduction plus convection ( $Cd+Cv$ ), electron cyclotron heating (ECH), and radiation (Rad). Power to the electrons from Ohmic heating and charge exchange and recombination are approximately equal in these discharges and small on these plots, so they are not shown. Figure 5 indicates that at low  $q_{\min}$ , electrons are the dominant loss channel, but as  $q_{\min}$  increases the electron transport improves and the ions become the dominant loss channel by a small amount. The ion to electron energy exchange and  $T_i/T_e$  decrease with  $q_{95}$  because  $T_e$  decreases less with  $q_{95}$  than  $T_i$  does. In the full 9-shot dataset,  $T_i/T_e$  from  $\rho \sim 0$  to  $\sim 0.7$  is minimized at intermediate values of  $q_{\min} \sim 1.4$ -1.6.

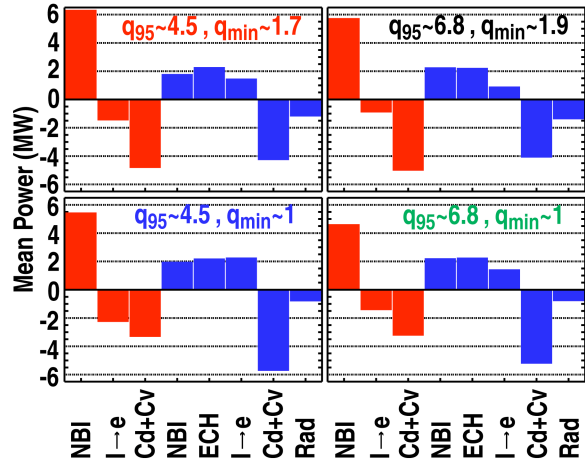


Fig. 5. Power balance of the scan endpoints.

#### IV. Comparison to Turbulence Measurements and Drift Wave Stability Analysis

In the absence of large-scale MHD, anomalous transport is usually attributed to drift-wave turbulence [7], typically low poloidal wave number ( $k_\theta$ ) ion temperature gradient modes, intermediate- $k_\theta$  trapped electron modes, and high- $k_\theta$  electron temperature gradient modes. In this view, the  $q$ -scaling of (i) turbulence measurements, (ii) calculations of drift wave growth rates, and (iii)  $\chi$ 's determined by power balance should all be consistent.

Figure 6 shows far infrared scattering (FIR) [8] measurements of line-averaged low- $k_\theta$  density fluctuation amplitudes versus time for the scan endpoints. Analysis time periods begin after  $t = 3$  s. These increase with  $q_{95}$  and even more so with  $q_{\min}$ , which is consistent

with the increase of  $\chi_i$  with  $q_{\min}$ , but not the decrease of  $\chi_e$  with  $q_{\min}$ . Intermediate and high- $k_\theta$  FIR measurements were below the noise levels so any differences are not discernible.

Drift wave linear stability analysis of the full dataset was performed using the trapped-gyro-Landau fluid (TGLF) model [9] at multiple radii. The TGLF code was given measured profiles as inputs to calculate the growth rate ( $\gamma$ ) and frequency of the most unstable mode at each  $k_\theta$ . Figure 7 shows low- and high- $k_\theta$  results at  $\rho=0.6$  for the scan endpoints. Flat lines in the low- $k_\theta$   $\gamma$ -plot are the local  $E \times B$  shear quench rates [10]. If this exceeds  $\gamma$  the mode may be stabilized. Positive/(negative) frequency is typically interpreted as an electron/(ion) mode.

The results are not universally consistent with the observed transport scalings. While ion and electron transport increases with  $q_{95}$ ,  $\gamma$ 's at all  $k_\theta$  decrease with  $q_{95}$ . Some high  $q_{95}$  cases with large  $\chi_i$  nonetheless have low- $k_\theta$   $\gamma$ 's less than the quench rate (e.g. the green curve in Fig. 7). These results also contradict the low- $k_\theta$  turbulence measurements. The low- $k_\theta$   $\gamma$ 's do increase with  $q_{\min}$ , in agreement with the observed increase of  $\chi_i$  with  $q_{\min}$ , but the high- $k_\theta$   $\gamma$ 's increase with  $q_{\min}$ , contrary to the observed decrease in  $\chi_e$  with  $q_{\min}$ .  $\gamma/k_\theta^2$  estimates the diffusivity due to these modes, and in all discharges it suggests intermediate and high- $k_\theta$  electron modes are irrelevant for transport compared to low- $k_\theta$  ion modes. This is at odds with the power balance showing electrons contributing significantly to total transport losses.

## V. Discussion and Conclusions

The unexpected decrease in electron transport and broadening of  $T_e$  with  $q_{\min}$  is perhaps beneficial for scenarios that seek to maximize bootstrap current with elevated  $q_{\min}$ . A caveat in this analysis is that there is evidence for anomalous transport of fast ions increasing with  $q_{\min}$ , but the fast ion transport was taken to be neoclassical. If this loss was underestimated in the higher  $q_{\min}$  discharges, then the ion transport may not increase as much with  $q_{\min}$ , and the electron transport may decrease more with  $q_{\min}$  than this analysis indicates. The inconsistency between the  $q$ -dependence of the linear stability analysis results and the observed transport

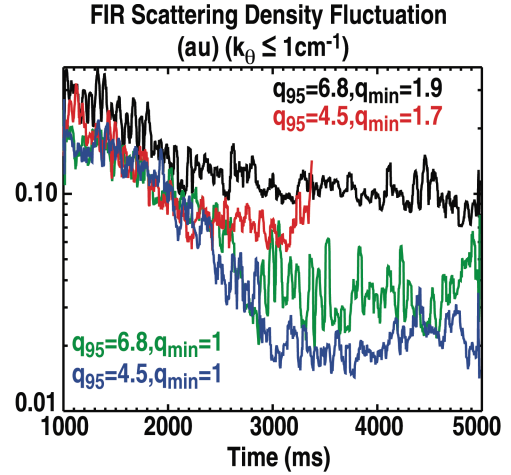


Fig. 6. FIR line-averaged low- $k$  density fluctuation measurements of the scan endpoints.

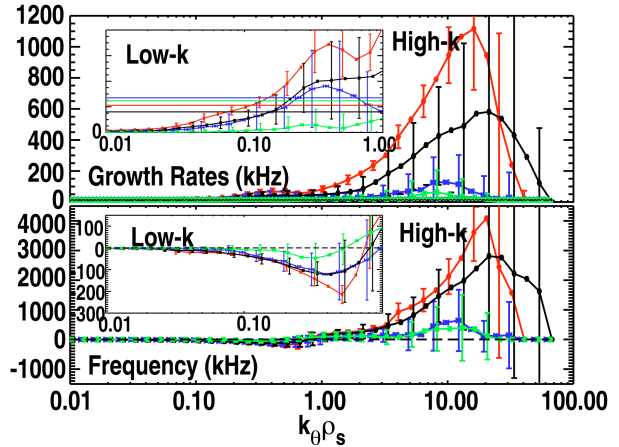


Fig. 7. Drift wave growth rate and frequency of the scan endpoints from TGLF linear stability analysis at  $\rho=0.6$ ; same color coding as Fig. 1 ( $\rho_s$  = ion gyroradius).

shows the need for nonlinear simulation to determine whether saturation due to mode coupling can explain the  $q$ -dependence.

This work was supported by the US Department of Energy under DE-AC52-07NA27344 and DE-FC02-04ER54698.

- [1] J.R. Ferron *et al.*, to be submitted to Nucl. Fusion
- [2] L.L. Lao *et al.*, Nucl. Fusion **30**, 1035 (1990).
- [3] B.W. Rice *et al.*, Phys. Rev. Lett. **79**, 2694 (1997).
- [4] A. Pankin *et al.*, Comput. Phys. Commun. **159**, 157 (2004).
- [5] O. Sauter *et al.*, Phys. Plasmas **6**, 2834 (1999).
- [6] H.E. St. John *et al.*, *Proceedings of the 15<sup>th</sup> International Conference on Plasma Physics and Controlled Nuclear Fusion Research*, Seville, Spain, 1994 (IAEA, Vienna, 1995), Vol. 3, p. 603.
- [7] E.J. Doyle *et al.*, Nucl. Fusion **47**, S18-S127 (2007).
- [8] C.L. Rettig *et al.*, Rev. Sci. Instrum. **61**, 10 (1990).
- [9] G.M. Staebler *et al.*, Phys. Plasmas, **14**, 055909 (2007).
- [10] J.E. Kinsey *et al.*, Phys. Plasmas, **15**, 055908 (2008).